Kinetics and Mechanism of Transitions Involving the Lamellar, Cubic, Inverted Hexagonal, and Fluid Isotropic Phases of Hydrated Monoacylglycerides Monitored by Time-Resolved X-ray Diffraction†

Martin Caffrey
Department of Chemistry, The Ohio State University, Columbus, Ohio 43210-1173
Received March 23, 1987; Revised Manuscript Received May 26, 1987

ABSTRACT: A study of the dynamics and mechanism of the various thermotropic phase transitions undergone by the hydrated monoacylglycerides monoolein and monoelaidin, in the temperature range of 20–120 °C and from 0 to 5 M NaCl, has been undertaken. Measurements were made by using time-resolved X-ray diffraction at the Cornell High-Energy Synchrotron Source. The lamellar chain order/disorder, lamellar/cubic (body centered, space group No. 8), cubic (body centered, No. 8)/cubic (primitive, No. 4), cubic (body centered, No. 12)/cubic (primitive, No. 4), cubic (primitive, No. 4)/fluid isotropic, cubic (body centered, No. 12)/inverted hexagonal, cubic (primitive, No. 4)/inverted hexagonal, and hexagonal/fluid isotropic transitions were examined under active heating and passive cooling by using a jump in temperature to effect phase transformation. All of the transitions with the exception of the cubic (body centered, No. 8)/cubic (primitive, No. 4) and the cubic (body centered, No. 12)/cubic (primitive, No. 4) cooling transitions were found (1) to be repeatable, (2) to be reversible, and (3) to have an *upper bound* on the transit time (time required to complete the transition) of ≤3 s. The shortest transit times recorded for the various phase changes in the heating direction were ≤1.9 (lamellar chain melting), ≤1.7 [lamellar liquid crystal/cubic (body centered, No. 8)], ≤0.5 [cubic (body centered, No. 8)/cubic (primitive, No. 4)], ≤0.9 [cubic (primitive, No. 4)/hexagonal], ≤1.3 [cubic (body centered, No. 12)/cubic (primitive, No. 4) and cubic (body centered, No. 12)/hexagonal], and ≤0.6 s (hexagonal/fluid isotropic). For the exceptions noted above, the transitions were slow with transit times ranging from 0.5 to 30 min and displayed pronounced hysteresis and/or undercooling. Regardless of the direction of the transitions, all but one appear to be two state to within the sensitivity limits of the time-resolved method. In the case of the lamellar liquid crystal/cubic (body centered, No. 8) transition a stable intermediate of unknown identity was apparent. In addition to the time-resolved measurements, data were obtained on the stability of the various phases in the temperature range of 20–120 °C and from 0 to 5 M NaCl. In the case of fully hydrated monoolein, high salt strongly favors the hexagonal over the cubic (body centered, No. 8) phase and slightly elevates the hexagonal/fluid isotropic transition temperature. With fully hydrated monoelaidin, the hexagonal phase which is not observed in the absence of salt becomes the dominant phase at high salt concentration. In this case, the cubic (body centered, No. 8)/cubic (primitive, No. 4) and lamellar liquid crystal/cubic (body centered, No. 8) transition temperatures decrease while that of the lamellar chain order/disorder transition increases with NaCl concentration. Structural parameters and thermal expansivity of the long spacings for the various phases as a function of salt concentration are presented.

In the past two decades, the equilibrium properties of lipid mesomorphic phases have been the subject of extensive investigations. It is only recently that the structural dynamics and mechanism of phase transformations have received attention. Time-resolved X-ray diffraction (TRXRD),[1] a method utilizing synchrotron-derived photons and a two-dimensional live-time X-ray imaging device, has proven particularly well suited to the latter types of investigations. It provides a direct means for acquiring mesomorphic structural information as a function of time. When the progress of a transition is tracked from beginning to end, details such as the presence of transient intermediate phases and their order of appearance and lifetimes can be determined. This, along with the kinetic data, provides an ideal framework upon which to model the transition mechanism. Once formulated, the mechanism, by virtue of its predictive powers, can be tested, evaluated, and refined by additional experimentation.

A knowledge of the mechanism of lipid-phase transitions is integral to our understanding of the structural and dynamic requirements for transitions that occur in biological systems, for example, during membrane fusion or fat digestion. Mechanisms have been proposed for such transitions that involve local alteration of the phase state of the component

† This work was supported by the National Institutes of Health (Grant DK36849) and by a Grant-in-Aid of Research from Sigma Xi, The Scientific Research Society.

[1] Abbreviations: a, length of the cubic unit cell edge; BCC8, body-centered cubic, space group No. 8 (*Im*3*m*, *I*432, *I*$\bar{4}$3*m*, *Im*3, *I*23, *I*2$_1$3); BCC12, body-centered cubic, space group No. 12 (*Ia*3*d*); CESR, Cornell Electron–Positron Storage Ring; CHESS, Cornell High-Energy Synchrotron Source; CP4, cubic primitive, space group No. 4 (*Pn*3*m*, *Pn*3); d, interlamellar spacing; d_l, lipid bilayer thickness; d_w, water layer thickness; DHPE, dihexadecylphosphatidylethanolamine; DOPE-Me, monomethylated dioleoylphosphatidylethanolamine; DPPC, dipalmitoylphosphatidylcholine; DSC, differential scanning calorimetry; EPR, electron paramagnetic resonance; FI, fluid isotropic phase; GeV, billion electron volts; H_{II}, inverted hexagonal phase; HEPES, 4-(2-hydroxyethyl)-1-piperazineethanesulfonic acid; *hkl*, the Miller–Bravais indices; keV, thousand electron volts; L_α, lamellar liquid crystal phase; MAG, monoacylglyceride; ME, monoelaidin; MO, monoolein; NMR, nuclear magnetic resonance; PC, phosphatidylcholine; PE, phosphatidylethanolamine; PLM, polarized light microscopy; $s = h^2 + k^2 + l^2$; $S_{obsd} = a^{-1}\sqrt{s}$; T_i and T_f, instantaneous and final sample temperatures, respectively; TLC, thin-layer chromatography; TRXRD, time-resolved X-ray diffraction; t_T, transit time. The lipid-phase notation used is that of Luzzati (1968).

0006-2960/87/0426-6349$01.50/0

Chart I

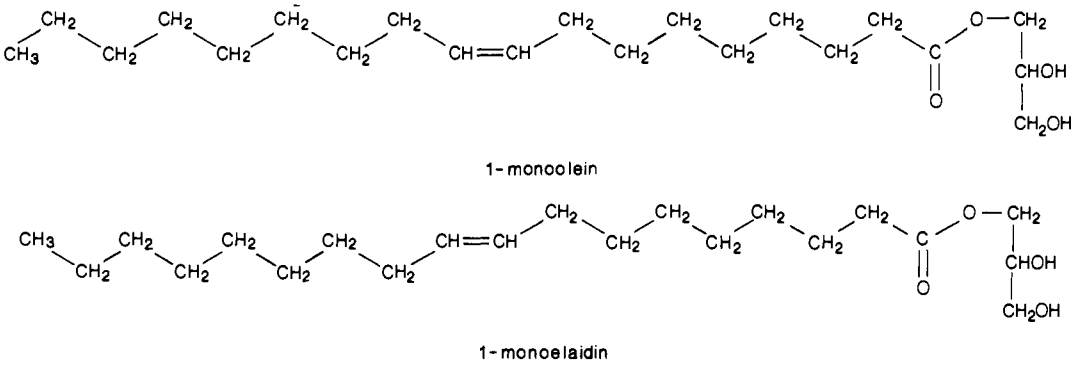

lipids. Comparing the rates of these vital physiological processes with those measured for bulk lipid-phase transformations provides a means for evaluating the proposed mechanisms.

This study represents another in a series designed to systematically establish the dynamics and mechanisms of the various lyotropic, thermotropic, and ionotropic phase transformations undergone by lipids and other liquid-crystalline materials. Thus far, the thermotropic chain-melting transition in the lamellar phase of dipalmitoylphosphatidylcholine (DPPC) and the lamellar gel/lamellar liquid crystal (L_α) and the lamellar/inverted hexagonal (H_{II}) phase transitions in phosphatidylethanolamine (PE) have been examined, the kinetics have been established, and a mechanism has been proposed for one of the bilayer/nonbilayer transformations (Caffrey & Bilderback, 1984; Caffrey, 1985). An earlier objective of the present study was to examine how lipid hydration modulates the structural dynamics of the various phase transitions undergone by the monoacylglycerides (MAGs) and in particular those involving the cubic phase. Because of difficulties encountered in preparing homogeneous samples at less than full hydration, an alternative approach of using high salt concentrations to effectively dehydrate the lipid was taken and measurements were performed in an excess aqueous phase with NaCl concentration ranging from 0 to 5 M. With the exception of two intercubic transitions which are slow, the results show that, regardless of the direction, salt concentration, and MAG identity and despite the changes in periodicity and in long- and short-range order, all transitions occurred with transit times (t_T, time required to complete a transition) of $\leq$3 s. In addition, the temperature/composition phase diagrams of the monoolein (MO)/NaCl and monoelaidin (ME)/NaCl systems (see Chart I for structures) have been established in the range of 20 to 120 °C from 0 to 5 M salt and the structural parameters of the various mesomorphic phases determined. The time-resolved results provide a basis for evaluating proposed mechanisms for the various mesomorphic phase transformations.

The MAGs were chosen for investigation because they exhibit mesomorphic phases with one-, two-, and three-dimensional periodicity and a fluid isotropic phase in an accessible temperature range. Furthermore, they are stable and available in high purity at low cost, and their phase properties have been the focus of considerable attention, presumably reflecting their importance as emulsifiers and as intermediates in lipid digestion and metabolism and their use in black lipid membrane studies (Pagano et al., 1973; Lutton, 1965; Krog et al., 1985; Patton & Carey, 1979).

Experimental Procedures

Materials. MO and ME obtained from Supelco (Bellefont, PA) and Nu-Chek-Prep (Elysian, MN), respectively, had a purity of $\geq$98% as judged by thin-layer chromatography of >100 μg of lipid in three solvent systems (chloroform/methanol/water, 65:25:4 v/v; petroleum ether/diethyl ether/acetic acid, 70:30:0.5 v/v; hexane/toluene/acetic acid, 60:40:1 v/v) each on two solid supports (Whatman K5F silica gel, Whatman; Adsorbosil Plus P Prekotes, Alltech) as previously described (Caffrey & Feigenson, 1981). All other chemicals and solvents were of reagent grade. Water was purified by using a Milli-Q (Millipore) system.

Sample Preparation. MAG dispersions were prepared by combining lipid with an excess of either water or buffer (0.1 M HEPES, pH 7.4) containing NaCl ranging up to 5 M. Homogeneous mixing was achieved by using a home-built device consisting of two disposable 1-mL tuberculin syringes connected at the Luer tip via a 5-mm length of plastic in which a 0.5-mm diameter hole had been drilled. Lipid was added to the device as a dry powder (ME) or as a liquid (MO at ~40 °C) upon which was layered the suspending aqueous phase. The system was flushed with argon, the plungers were inserted into the syringe barrels, and the mixture was passed under pressure from one syringe to the other through the interconnecting constriction by working the two plungers back and forth. The samples were then transferred to thin-walled (10-μm) quartz or glass capillaries (1-mm internal diameter, Supper). With ME, pelleting to the bottom of the capillary was achieved by centrifugation (International Clinical Centrifuge, Model 1528E) at maximum speed in a swinging bucket rotor. MO proved more difficult to handle, invariable requiring use of a 25-μL Hamilton microsyringe plunger to force the hydrated lipid into the narrow end of the capillary. To ensure that the lipid was at all times surrounded by an excess of aqueous medium, a 10-μL volume of the suspending solution was centrifuged into the capillary and into contact with the lipid when loading was complete. In the case of T-jump experiments of the type described below, it is important to position the lipid securely at the bottom of the capillary. Failure to do so can result in argon (vide infra) being trapped in this region, expanding rapidly during the T jump and displacing the lipid out of the interrogating X-ray beam. Subsequent to loading, the capillary was flushed with argon, flame-sealed, and hermetically sealed with two applications of a 5-min epoxy (Harduron Inc.). Where possible, sample homogeneity was ascertained by examining the live-time imaged diffraction pattern as the sample capillary was translated vertically and horizontally through the X-ray beam. Inhomogeneous samples were easily identified as having various phase types or lattice parameters within a given phase at a fixed temperature in different regions of the sample.

Sample temperature was monitored by positioning a thermocouple (copper/constantan, Teflon covered, 0.003-in. diameter, Omega) either inside and close to the bottom of the

sample capillary embedded in the lipid sample or alternatively outside the capillary in the air stream but as close (within 2 mm) as possible to the X-ray beam. For samples with the thermocouple actually inside the capillary, the thermocouple leads were sealed to the capillary wall with 5-min epoxy.

X-ray Diffraction. (*A*) *X-ray Source and Camera.* Most of the diffraction experiments were carried out by using wiggler-enhanced, monochromatic (0.157-nm), focused X-rays on the Al line at CHESS as previously described (Caffrey, 1985) with the following modifications. A 10 cm long cylindrically bent asymmetric crystal of germanium (111) was used for monochromatization and horizontal focusing. Higher order harmonics were eliminated, and the beam was vertically focused by total reflection of the fixed energy beam from a 60 cm long platinum- or nickel-coated mirror. These optics enabled focusing of the beam to a point approximately 1.5 mm wide and 0.3 mm high on the front face of the detector and provided 3×10^{10} photons/s down a 0.3-mm diameter collimator (Supper) with CESR operating at 5.2 GeV and 30 mA total of electron beam current in the three-bunch mode and the six-pole wiggler at half-power.

X-radiation damage to the samples was minimized by implementing the precautions outlined earlier (Caffrey, 1984). To this end, a standard protocol was adopted which involved moving to a new part of the sample at least every second or third temperature scan or *T*-jump experiment. Where slow temperature scans were of long duration, a computer-controlled beam shutter was used that cycled 2 s open, 5 s closed.

Static and time-resolved X-ray diffraction measurements were made by using either a Buerger Precession Camera (Supper) or a homemade low-angle X-ray diffraction camera with a 0.3-mm diameter collimator. The latter incorporates a 1 m long optical bench (X-95, Klinger), with the following components on adjustable carriers: computer-controlled beam shutter, collimator, low-power (10–20× magnification) crystal viewing microscope with cross hairs for sample alignment viewed from below, FTS gas crystal heating/cooling device, eucentric goniometer (large and small, motorized, Supper) on a Huber stage in turn mounted on a computer-controlled, motorized horizontal translation stage, beam stop, film cassette, and carriage for the X-ray imaging device. The latter incorporates a three-stage image intensifier tube (Varo) operated at 5–7 V and a video camera, typically a Cohu (Model 5272-2220/AL4) fitted with an Apollo f0.85, 25-mm lens (Comprehensive Video Supply Corp., Northvale, NJ 07647) and mounted at a 90° angle with respect to the image intensifier. The enhanced X-ray image from the intensivier tube was viewed via the camera by using a front-surfaced mirror positioned at a 45° angle with respect to the optical axis of both intensifier and camera. With this arrangement it was possible to quickly interchange the static and time-resolved detection systems and to choose sample-to-detector distances anywhere from 2 to 80 cm. The cameras were mounted on a home-built optical table.

(*B*) *Static X-ray Diffraction.* Diffraction patterns were recorded on X-ray sensitive film (CEA Reflex 25, CEA America Corp.; DEF5, Kodak, Rochester, NY) as previously described (Caffrey, 1985). Sample temperature was controlled by using a forced-air crystal heating/cooling apparatus (FTS). The air stream was coaxial with the sample capillary, and sample temperatures from −60 to 80 °C were accessible with control to ±1.5 °C. Exposure times varied from 30 s to 15 min depending on beam current, sample-to-detector distance, sample composition, and mesomorphic phase type. X-ray wavelength was determined by using a lead nitrate standard (0.3-mm diameter capillary; *International Tables for X-ray Crystallography*, 1968) and a carefully measured sample-to-film distance.

(*C*) *Time-Resolved X-ray Diffraction.* A complete description along with performance characteristics of the system used for TRXRD may be found in the following references: Caffrey and Bilderback (1984), Caffrey and Feigenson (1984), and Caffrey (1985). The essential components are an X-ray camera (described above), a two-dimensional, live-time X-ray imaging device, a character generator interfaced to a digital voltmeter (thermometer), an electronic clock, and a video camera, recorder, and monitor. Quantitative diffracted intensity and position information was obtained by digital processing of the live-time diffraction patterns recorded on video tape as previously described (Caffrey, 1985). Except for frame averaging, the raw, uncorrected data are presented in this communication.

The MAG/NaCl temperature–composition phase diagrams were determined by using the time-resolved system in conjunction with the forced-air crystal heater/cooler below 20 °C and the temperature-jump device (vide infra) above this temperature. Thus, diffraction was recorded in live time as sample temperature was changed either stepwise manually or in slow-scan (5–10 °C/min) mode by using the programmable temperature controller (Caffrey, 1985). Sample temperature, elapsed time, and the two-dimensional live-time diffraction image were recorded simultaneously on video tape throughout the *T*-scan measurement. Mesomorphic phase identification was based on both low- and wide-angle diffraction, and changes in diffraction behavior indicated a phase boundary. Heating and cooling scans were performed in like manner.

In order to rapidly adjust sample temperature from that of ambient to some predetermined value, a previously described *T*-jump apparatus was used (Caffrey, 1985). This device consists of a temperature-regulated heat gun which is solenoid activated to rapidly deflect a hot air stream onto or away from the sample capillary centered in and coaxial with the air stream. Cooling occurred passively in air when a second solenoid was activated to deflect the heat gun air stream away from the sample.

Results

Effect of Salt Concentration on Monoacylglyceride Mesomorphic Phase Behavior. Before kinetic measurements are carried out, it is imperative that the underlying equilibrium thermotropic phase relations of the system be established. To this end, the effect of NaCl concentration on MAG phase behavior in excess 0.1 M HEPES, pH 7.4, was determined. Both TRXRD and static X-ray diffraction were used to establish phase identity and phase boundaries as a function of temperature. As is evident from the data presented in Figure 1, a major advantage of the TRXRD method is that phase identification is made continuously as a function of temperature and the likelihood that a phase which exists over a narrow temperature range goes undetected is minimized.

(*1*) *Monoolein.* In the absence of NaCl, fully hydrated MO undergoes a cubic (primitive, space group No. 4, CP4) to inverted hexagonal (H_{II}) and a H_{II} to fluid isotropic (FI) phase transition at 85 and 106 °C, respectively, in the heating direction (Figure 1A). The H_{II} phase is stabilized at high salt concentration as evidence by a monotonic decrease in the CP4-to-H_{II} phase transition temperature to 25 °C at 5 M NaCl. In contrast, the FI phase is destabilized, but only slightly, by high salt concentration, and at 5 M NaCl the H_{II}-to-FI transition temperature has increased to 109 °C. Thus, while in the absence of NaCl the H_{II} phase exists over

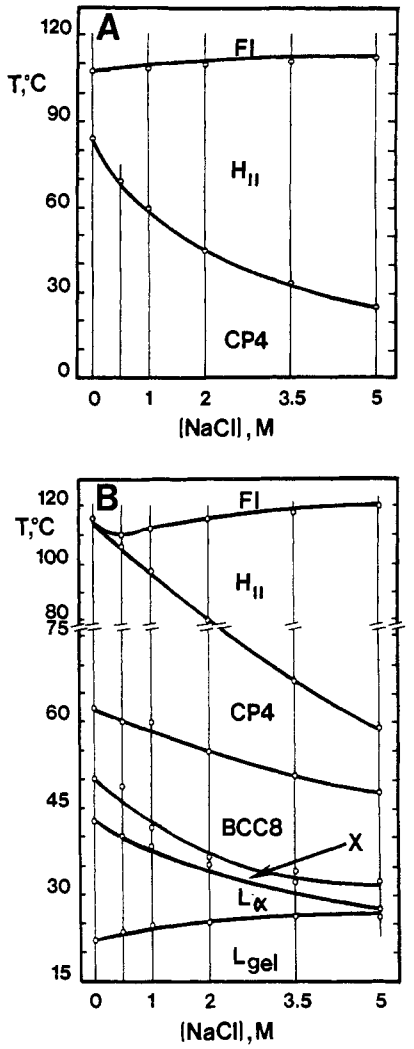

FIGURE 1: Mesomorphic phase properties of aqueous dispersions of monoolein (A) and monoelaidin (B) as a function of temperature and NaCl concentration determined by a combination of static and time-resolved X-ray diffraction. Phase type and boundaries were determined continuously upon sample heating at a rate of 5–10 °C/min. Samples were dispersed in 0.1 M Na-HEPES, pH 7.4, at the indicated NaCl concentrations as described under Experimental Procedures. The vertical lines in the phase diagram indicate the isopleths studied and serve to emphasize one of the advantages of the time-resolved X-ray diffraction method, namely, that measurements can be made continuously along a given isopleth over the full temperature range indicated.

a 20 °C range, at 5 M NaCl it is the dominant phase spanning an 84 °C temperature range.

In one experiment carried out with MO in 0.1 M HEPES, pH 7.4, it was found that the CP4 phase persisted down to −18 °C in the presence of an undercooled aqueous medium. At −18 °C freezing of water appeared to trigger conversion to a crystalline lamellar phase, which persisted on heating to 17 °C, at which point it transformed to the CP4 phase. It is conceivable that the behavior of the CP4 phase upon cooling represents the undercooling phenomenon and that ice formation simply acts to nucleate the low-temperature phase. It is also possible that the subzero cooling transition is lyotropic in origin and is initiated by freeze dehydration. Similar observations have been made with hydrated dioleoylphosphatidylserine (Caffrey, 1987a).

In addition to MO dispersions in HEPES buffer, TRXRD measurements were also performed on MO in excess water. In this case, the stable room temperature phase was found to be the cubic (body centered, space group No. 8, BCC8), which transforms upon heating to the CP4 and subsequently to the H_{II} and FI phases. In one experiment it was found that when the BCC8 phase was cooled to below 0 °C, the lipid underwent a liquid crystal to gel phase change in the presence of undercooled water as evidenced by the appearance of two sharp wide-angle reflections in the live-time imaged diffraction pattern. Continued cooling led to ice crystal formation. Interestingly, the recalescent heat was sufficient to "melt" the gel-phase lipid. Continued cooling restored the gel phase in the presence of ice. While not immediately relevant to the topic at hand, to my knowledge, this is the first example of where heat liberated upon ice crystal formation effected a lipid mesomorphic phase change.

(*2*) *Monoelaidin.* The phase behavior of fully hydrated ME in the absence of added NaCl is quite complex, as shown in Figure 1B. With increasing temperature the following sequential phase transformations occur: lamellar gel → L_α → BCC8 → CP4 → FI. All, except for the L_α-to-BCC8 transition, are sharp and well-defined. In the latter case, as temperature is increased, the L_α phase slowly fades and a series of extremely low angle lines appear in the diffraction pattern from which evolve reflections characteristic of the BCC8 phase. The exact nature of this intermediate phase is unknown and was not examined further in this study.

The addition of salt was found to have a slight destabilizing effect on the lamellar gel phase of ME in that the chain-melting transition increased slightly from 22 to 25 °C at 0 and 5 M NaCl, respectively (Figure 1B). In contrast, high salt stabilized the BCC8 and the CP4 phases. However, the most profound effect was seen at higher temperatures where an H_{II} phase, not previously seen in the absence of salt, was expressed and became the dominant phase at 5 M NaCl. Interestingly, low concentrations of salt up to 0.5 M favored the FI over the H_{II} phase. As salt increased beyond this concentration however, the H_{II}-to-FI transition temperature rose to a final value of 118 °C at 5 M NaCl.

Structural Parameters. The equilibrium thermotropic phase properties of the MO and ME systems having been established, the next task was to determine structural parameters of the various mesomorphic phases as a function of temperature and salt concentration. To this end, static diffraction patterns were recorded on X-ray-sensitive film. The results are presented in Table I. In the case of MO and magnitude of the long spacing in all three phases, CP4, H_{II}, and FI, decreased with salt concentration. Since the exact composition of each phase is not known and since the long-spacing value represents a composite of lipid and aqueous phase dimensions, the manner in which salt influences these two compartments within a given mesomorphic phase cannot be resolved at this time.

In all of the MO phases, and over the entire temperature range examined, the wide-angle region of the diffraction patterns revealed a diffuse scattering peak centered at ca. (0.46 $nm)^{-1}$, indicating that the lipid acyl chains are in the "fluid" or disordered state. The corresponding low-angle diffraction patterns are presented in Figure 2. As shown in Table II, the cubic (primitive) phase has been tentatively indexed on a space group No. 4 lattice (CP4). In the best case, a total of 11 diffraction lines were indexed to a resolution of 2.0 nm for MO in the absence of added NaCl.

Additional cubic modifications of MO are included in Table II. These include BCC8 and a body-centered cubic phase with space group aspect No. 12 (BCC12). As noted in footnote *b* to Table II, all space group assignments in this study are tentative. While some of the samples were strongly diffracting with up to 11 reflections clearly defined, this number was still

Table I: Structural Parameters of the Different Mesomorphic and Fluid Isotropic Phases of Monoolein and Monoelaidin in Excess 0.1 M HEPES, pH 7.4[a]

NaCl concn (M)	lamellar gel d_{001} (nm)	lamellar liquid crystal d_{001} (nm)	cubic body centered No. 8 d_{110} (nm)	cubic primitive No. 4 d_{110} (nm)	inverted hexagonal $2d_{11}$ (nm)	fluid isotropic (nm)
			Monoolein			
0				6.95 (13)[b]	5.44 (95)	4.26 (115)
2				6.37 (13)	4.99 (94)	4.03 (115)
3.5				6.26 (13)	4.82 (95)	
5					4.72 (95)	3.85 (116)
			Monoelaidin			
0	6.28 (15)[c]	5.40 (30)[c]	11.50 (52)	6.15 (75)	5.53 (105)	4.5 (115)
1	6.24 (15)	5.50 (30)	10.67 (50)	5.75 (76)	5.81 (77)	4.4 (115)
3.5	6.24 (15)		15.00 (30)[d]	5.83 (61)		4.1 (120)
			9.95 (44)			

[a] All measurements were made in the heating direction with the one exception denoted by footnote *d*. [b] Temperature values are given in parentheses in °C. [c] The corresponding wide-angle X-ray diffraction peaks were 0.420 and 0.427 nm for the lamellar gel phase and 0.45 nm (diffuse) for the lamellar liquid crystal phase. [d] This measurement was made in the metastable, undercooled condition.

Table II: Cubic Space Group Assignments for Aqueous Dispersions of Monoolein and Monoelaidin[a]

space group assignment[b]	lipid type[c]	long-spacing ratio	no. of absent reflections[d] for cubic space group aspect: primitive, No. 2	4	5	6	7	body centered, No. 8	10	11	12	face centered, No. 17
BCC8	monoelaidin	$1:\sqrt{2}:\sqrt{3}:\sqrt{5}:\sqrt{7}:\sqrt{9}$	9	7	6			3				≥9
CP4	monoelaidin	$\sqrt{2}:\sqrt{3}:\sqrt{4}:\sqrt{6}:\sqrt{8}:\sqrt{9}$	1	0			6		1			1
BCC12	monoolein	$\sqrt{3}:\sqrt{4}:\sqrt{7}:\sqrt{8}:\sqrt{10}:\sqrt{11}:\sqrt{12}:\sqrt{13}$								1	0	
BCC8	monoolein	$1:\sqrt{2}:\sqrt{3}:\sqrt{5}:\sqrt{6}:\sqrt{7}:\sqrt{8}:\sqrt{9}:\sqrt{10}:\sqrt{11}:\sqrt{12}$	9	7		2		1				≥8
BCC8	monoolein	$1:\sqrt{2}:\sqrt{3}:\sqrt{5}:\sqrt{6}:\sqrt{7}:\sqrt{9}:\sqrt{12}$	12	10		5		4				≥8
CP4	monoolein	$\sqrt{2}:\sqrt{3}:\sqrt{4}:\sqrt{6}:\sqrt{9}:\sqrt{10}:\sqrt{11}:\sqrt{12}:\sqrt{14}:\sqrt{17}$	3	1								
CP4	monoolein	$\sqrt{2}:\sqrt{3}:\sqrt{4}:\sqrt{6}:\sqrt{8}:\sqrt{9}:\sqrt{10}:\sqrt{12}$	2	1					2			

[a] The table lists the ratio of the positions of the low-angle reflections in the diffraction patterns and the number of reflections missing from each pattern if it is to conform completely to the permitted reflection profile of a particular space group. [b] Space group assignment is necessarily tentative since in no instance was there a sufficient number of reflections for a completely unique identification. In the case of the CP4 assignment for monoelaidin, an identical set of reflections with a similar intensity distribution was obtained at 0 and 1 M NaCl with corresponding d_{110} spacings of 6.15 and 5.75 nm. This lends credence to the CP4 assignment since it is unlikely that missing reflections in the other possible space groups would remain at zero intensity due to a fortuitous distribution of matter in the unit cell as its dimensions change by this amount. In all cases the particular space group assigned corresponds to that with the least number of missing reflections. [c] Lipids were dispersed in either Milli-Q water or 0.1 M HEPES, pH 7.4, with or without added salt. [d] The number of absences is based on an evaluation of reflections with $1 \leq s = h^2 + k^2 + l^2) \leq 68$ (*International Tables for X-ray Crystallography*, 1968).

not sufficient for a unique identification. Alas, the situation does not improve with the TRXRD measurements because of the finite size and limited spatial resolution of the detector. Thus, many of the phase assignments made in the course of the dynamic studies were based upon simultaneous static measurements on X-ray film and on experience gained in recognizing phases by visually comparing real-time video images and static X-ray photographs.

The long spacings and, where appropriate, the short spacings of the various phases in hydrated ME as a function of salt concentration are listed in Table I. As is evident from the data in Figure 1B, the mesomorphic behavior of ME is very sensitive to salt concentration, and so it was not possible to record patterns in a single-phase region over the entire range of salt concentration at a single temperature. As a result, the corresponding temperatues at which the measurements were made are listed next to the *d*-spacing value in Table I. As noted above, there are two cubic modifications discernible in hydrated ME both with and without added NaCl. The low-temperature modification indexed according to a body-centered lattice, space group No. 8 (BCC8, Table II). The high-temperature form indexed on a primitive cubic lattice, space group No. 4 (CP4), as was observed for the cubic phase of hydrated MO.

The low-temperature phase of fully hydrated ME is of the lamellar gel type in that the low-angle diffraction lines index on a lamellar lattice while the wide-angle region contains two sharp reflections at 0.420 and 0.427 nm with a visually estimated intensity ratio of >10:1. Since, strictly speaking, this is not an L_β phase in the notation of Luzzati (1968) and since the tilt angle of the acyl chains was not determined, hereafter this phase will be referred to simply as the lamellar gel phase.

Temperature-Scan Progress Curves. To indicate how the various phases evolve as sample temperature is slowly changed (*T*-scan mode), progress curves have been prepared that show the position in reciprocal space of X-ray diffraction lines observed in each phase of a function of temperature. The two-dimensional diffraction data were recorded in live time on video tape and serve to illustrate the structural connectivities or otherwise along with the thermal lattice coefficients of the different mesomorphic phases. The data have not been corrected for detector distortion previously characterized as being of the pincushion type (Caffrey & Bilderback, 1983).

In the case of MO at 2 M NaCl, there exists a reciprocal dependence of lattice size on temperature throughout most of the cubic and H_{II} phase region (Figure 3A). Some 5–10 °C below the transition to the H_{II} phase the CP4 phase lattice size levels out. Since temperatures in excess of 120 °C were not explored, the thermal sensitivity of the FI phase was not determined. Upon cooling, the reverse process was observed (data not shown) with phase coexistence evident in the transition regions. In all cases examined, there existed a 5–10 °C undercooling and/or hysteresis that was not carefully studied. At both the cubic/H_{II} and the H_{II}/FI transitions, sharp discontinuities were observed in the positions of the corresponding diffraction lines and/or scattering peaks. This is in contrast to the observations of Lindblom et al. (1979) with hydrated 1-monostearin wherein a continuity between the *d*(001) line

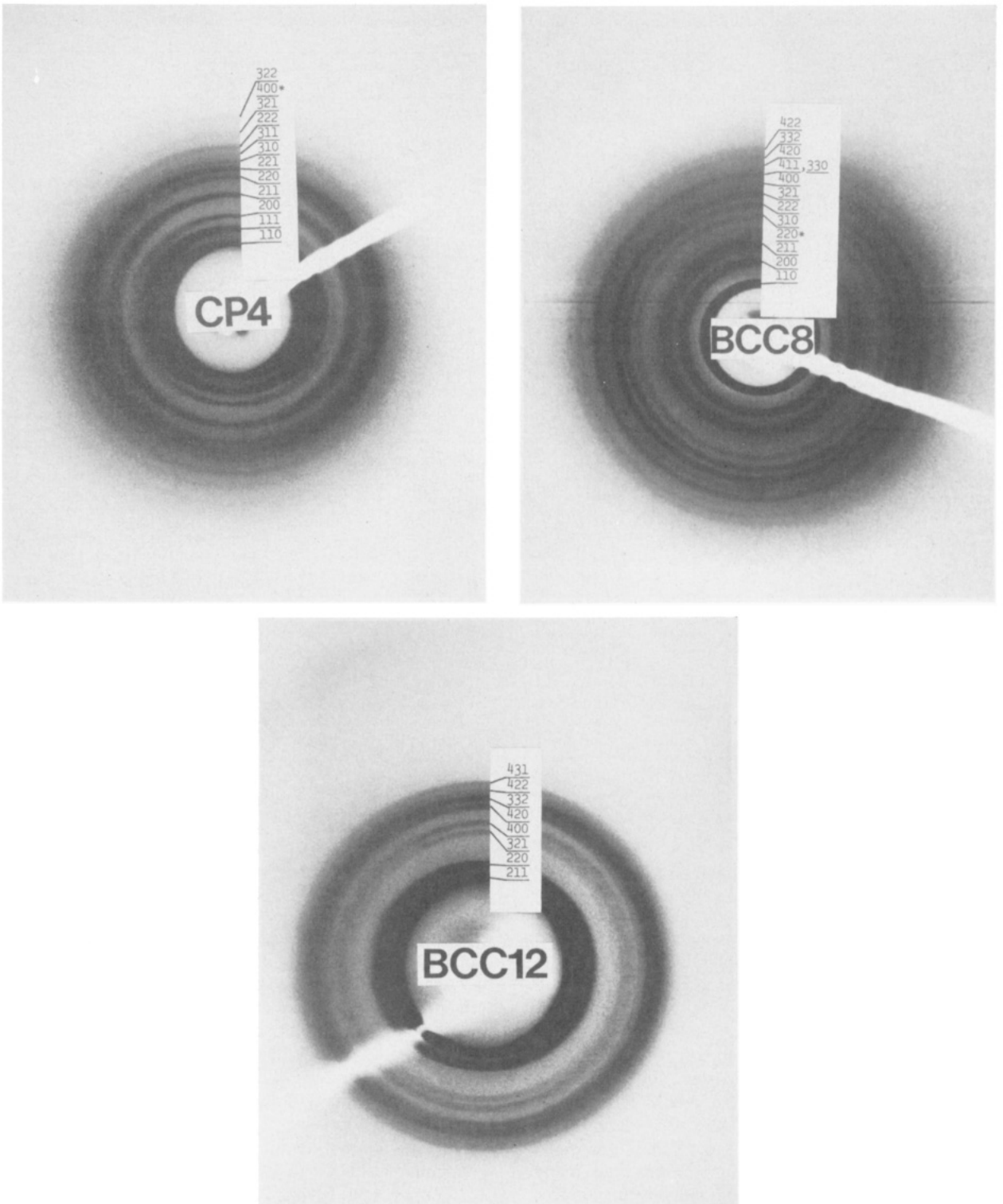

FIGURE 2: X-ray diffraction patterns of the three cubic modifications observed with hydrated monoolein: CP4, cubic primitive, space group No. 4 (*Pn*3*m* or *Pn*3), 20 °C; BCC8, cubic body centered, space group No. 8 (*Im*3*m*, *I*432, $I\bar{4}3m$, *Im*3, *I*23, $I2_13$), 24 °C; BCC12, cubic body centered, space group No. 12 (*Ia*3*d*), 28 °C. Miller–Bravais indices are shown, and permitted reflections not obvious in the original diffraction pattern are identified by an asterisk.

of the lamellar liquid crystal phase and the $d(222)$ line of the cubic (body-centered) phase was noted.

The *T*-scan curve for fully hydrated ME in the absence of added NaCl from 20 to 115 °C encompasses the lamellar gel, L_α, BCC8, CP4, and FI phases (Figure 3B). Sharp discontinuities are noted in the position of the diffraction lines at each of the transitions as observed above for MO. However, at the L_α/BCC8 transition unidentified intermediates displaying very low angle diffraction intervene as noted previously. In all cases excepting the lamellar gel and FI phases where limited data are available, lattice size decreases with increasing temperature. The reverse process occurs upon cooling at least into the CP4 phase.

At the high-temperature end of the CP4 phase the diffraction pattern becomes extremely spotty and remains so regardless of the direction of change in temperature or MAG identity. In contrast, a continuous powderlike pattern was obtained in the low-temperature end of this phase field. Thus,

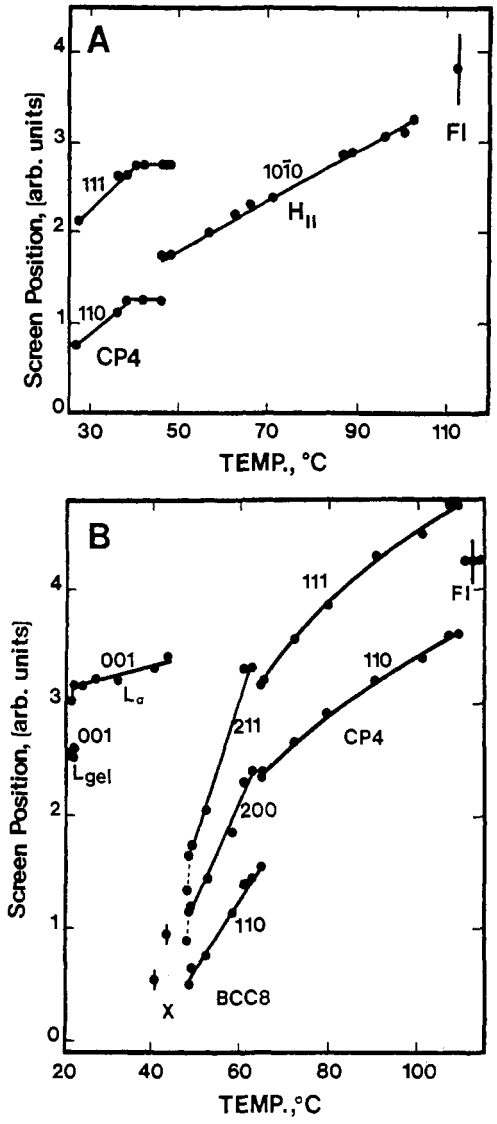

FIGURE 3: Changes in the diffraction pattern from aqueous salt dispersions of monoolein (A) and monoelaidin (B) during the course of a temperature scan experiment. Monoolein was dispersed in excess 2 M NaCl and 0.1 M HEPES, pH 7.4, and monoelaidin in excess 0.1 M HEPES, pH 7.4. Screen position refers to the position of the various diffraction lines measured directly from the video screen and corresponds to the position in reciprocal space. Screen position measurements and origin are arbitrary. The various mesomorphic phases are identified along with the Miller–Bravais index for each reflection. The vertical lines associated with the X and fluid isotropic (FI) phases indicate that the reflections from these phases are diffuse; the length of the line is proportional to the width of the peak.

assembly of the lipid into large crystallites is apparently facilitated at higher temperatures and/or by proximity to the phase transition region. It is also interesting to note that as the transition temperature is approached from below, the mobility of these cubic-phase crystallites dramatically increases as evidenced by the enormous diffracted intensity fluctuations observed in individual spots. This holds true regardless of whether the CP4 phase is transforming to the FI or the H_{II} phase. The newly formed H_{II} phase, however, does not possess this same degree of spottiness and is considerably more powderlike in appearance. Slow cooling from the FI phase, however, can give rise to a spotty H_{II}-phase diffraction pattern.

Kinetic Measurements. The kinetic measurements described below primarily concern phase transitions undergone by MO and ME dispersed in an excess aqueous phase with and without added NaCl. The transitions include the lamellar gel/L_α, L_α/BCC8, BCC8/CP4, CP4/H_{II}, H_{II}/FI, CP4/FI,

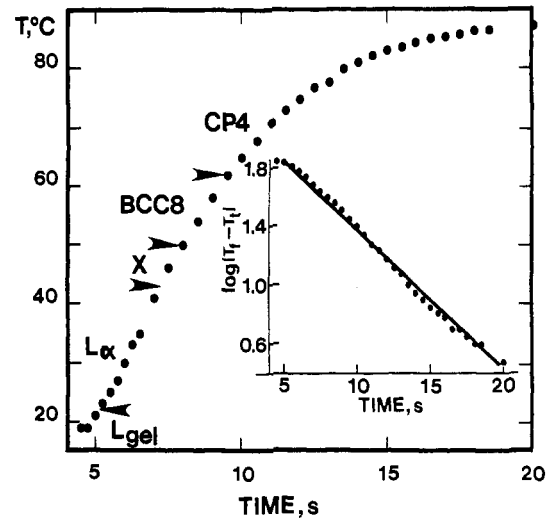

FIGURE 4: Sample temperature change with elapsed time after commencement of heating following a jump in temperature from 19 to 95 °C. Measurements were made with the thermocouple positioned inside the 1-mm diameter sample capillary containing monoelaidin in an excess of 100 mM HEPES, pH 7.4, and next to the X-ray beam. The insert shows the data plotted as log ($T_f - T_t$) vs. elapsed time, where T_f and T_t correspond respectively to final and instantaneous sample temperatures. Arrowheads indicate the position in time and temperature of the various phase transitions.

BCC12/CP4, and BCC12/H_{II}. As noted above under Structural Parameters and reemphasized here, cubic phase identification is tentative. Throughout the measurements, heating was active in the sense that heat was applied continuously to raise sample temperature while cooling was passive, occurring in air upon removal of the heat source.

During the kinetic measurements sample temperature was monitored continuously by using a thermocouple positioned either in or outside the capillary next to the X-ray beam. The thermal responsivity of the thermocouple ($\geq$170 °C·s^{-1}) has been previously described (Caffrey, 1985). With the thermocouple positioned in the sample, a heating curve showing sample temperature vs. elapsed time of the type shown in Figure 4 was obtained with hydrated ME following a jump in temperature from 30 to 95 °C. The positions in time of the various transitions undergone during this T-jump are indicated. Of note is the absence of thermal halts in the heating curve. This is in contrast to the heating curve for hydrated dihexadecylphosphatidylethanolamine (DHPE) in which a pronounced halt was observed at the chain-melting transition (Caffrey, 1985). The absence of a halt must surely indicate that the enthalpy change associated with the various monoelaidin transitions is much less and/or that the transition temperature range is broader than that of the aforementioned transition in DHPE. Furthermore, the linearity of the heating curve plotted as log ($T_f - T_t$) vs. elapsed time suggests qualitatively at least that the specific heats of the various bilayer and nonbilayer phases are similar [see Caffrey (1985)].

TRXRD data obtained with an aqueous dispersion of ME are presented in Figures 5 and 6. Raw data in the form of two-dimensional low-angle diffraction images and how these change with time and temperature during and after an applied T-jump are presented in Figure 5. The reverse process upon cooling is omitted due to space limitation, but these follow a similar pattern with slight differences arising from undercooling and/or hysteresis effects as will be described below.

The quantitative low-angle diffracted intensity information obtained by image processing and how this changes following the T-jump are presented in Figure 6. In this example the progress of ME in excess 0.1 mM HEPES, pH 7.4, through

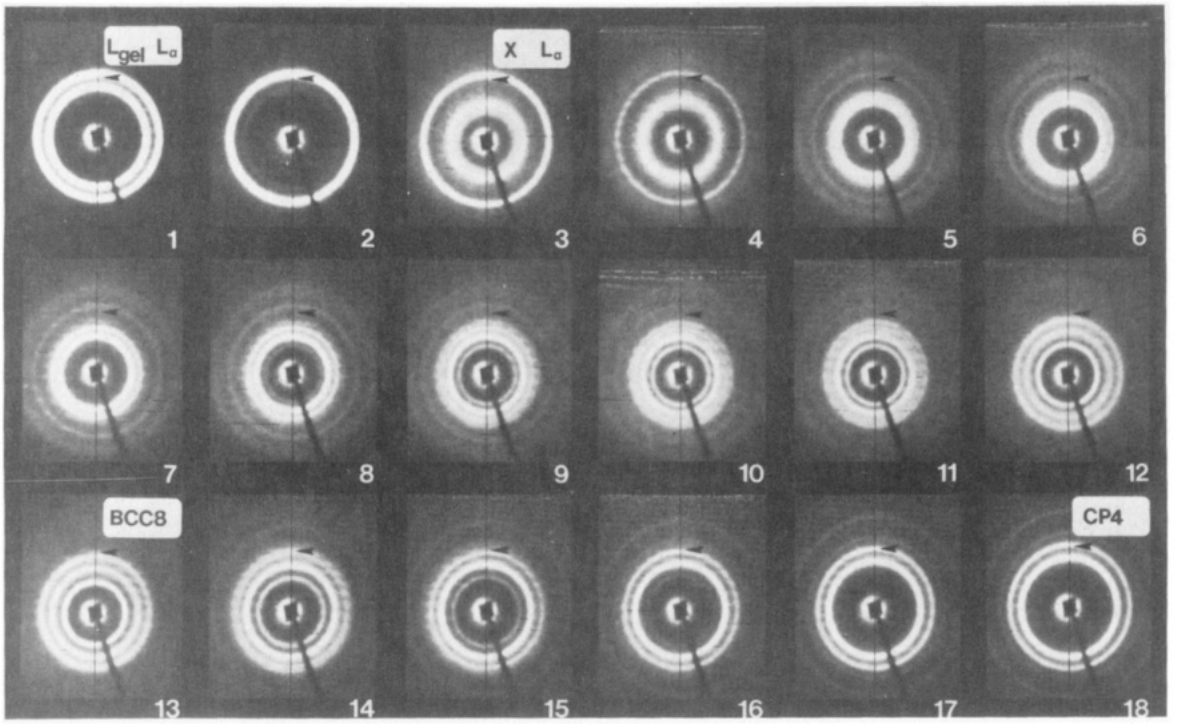

FIGURE 5: Dynamics of transitions involving the lamellar gel, lamellar liquid crystal, intermediate X, cubic (body centered, No. 8), and cubic (primitive, No. 4) phases in fully hydrated monoelaidin following a jump in temperature from 25 to 70 °C. Low-angle diffraction corresponding to the lamellar gel (001), lamellar liquid crystal (001), cubic (body centered, No. 8) (110), (200), and (211), and cubic (primitive, No. 4) (110), (111), (200), and (211) reflections was recorded by using the time-resolved X-ray diffraction method. Each photograph in this composite represents a single frame (33 ms) of the video-recorded live-time images. Elapsed time and corresponding sample temperature after the commencement of heating are as follows: (1) 8.5 s, 24 °C; (2) 10.2 s, 36 °C; (3) 12.1 s, 45 °C; (4) 12.4 s, 46 °C; (5) 12.7 s, 50 °C; (6) 12.7 s, 52 °C; (7) 13.9 s, 53 °C; (8) 14.6 s, 55 °C; (9) 15.4 s, 57 °C; (10) 15.9 s, 58.5 °C; (11) 16.1 s, 59 °C; (12) 17.5 s, 62 °C; (13) 18.1 s, 63 °C; (14) 19.7 s, 65 °C; (15) 20.7 s, 66 °C; (16) 21.8 s, 66.5 °C; (17) 24.1 s, 68 °C; and (18) 71.1 s, 70 °C. The arrowhead is included as a reference point.

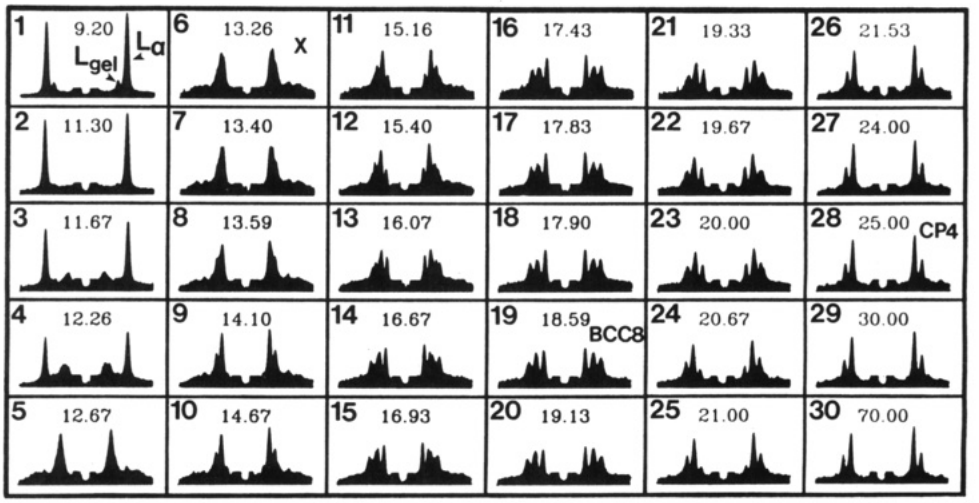

FIGURE 6: Kinetics of the lameller gel/lamellar liquid crystal, lamellar liquid crystal/intermediate X/cubic (body centered, No. 8), and cubic (body centered, No. 8)/cubic (primitive, No. 4) transitions undergone by fully hydrated monoelaidin in 0.1 M HEPES, pH 7.4, following a jump in temperature from 25 to 70 °C. Low-angle X-ray diffraction was recorded in live time and image processed to obtain diffracted intensity profiles as described under Experimental Procedures. Profiles were obtained from images representing the average of three video frames (equivalent to 100 ms at 30 frames/s). Elapsed time in seconds is indicated in each sequentially numbered frame.

the various mesomorphic phase states following a jump in temperature from ca. 25 to 70 °C is reported. The first frame at 25 °C shows the L_α phase coexisting with a small amount of residual lamellar gel phase just prior to initiating the *T*-jump. In the next two frames immediately following the *T*-jump perturbation, the lamellar gel phase disappears completely and the pattern is now dominated by the L_α phase accompanied by some low-angle scattering due to an, as yet, unidentified intermediate. The intensity distribution in the diffraction pattern from this intermediate changes with time at the expense of the L_α phase, which fades and eventually disappears (Figure 6-6). From this continuously changing intermediate (Figure 6-3 to -15) evolves the BCC8 phase with its characteristic three-line pattern (Figures 2 and 6-19). With time and continued heating the BCC8 phase is replaced by the CP4 phase, which at the final temperature of 70 °C is the only phase present (Figure 6-30) as expected from the temperature–composition phase diagram in Figure 1B. While not included in this sequence, the CP4/FI phase transition presents no surprises. It proceeds in like manner to the lower tem-

Table III: Transit Time of Various Thermotropic Phase Transitions Undergone by Aqueous Dispersions of Monoolein in Response to a Temperature Jump[a]

aqueous phase[b]	temperature jump[c] (°C)	transit time[d] (s)							
		cubic (BC8)	cubic (P4)	inverted hexagonal	fluid isotropic	cubic (BC12)	cubic (P4)	cubic (BC12)	inverted hexagonal
HEPES	90, heat		3.4						
HEPES	90, cool		2.1						
HEPES[e]	100, heat		1.6 ± 0.3			1.3			
HEPES[e]	100, cool		2.8 ± 0.8			34			
HEPES	110, heat		1.5 ± 0	1.9					
HEPES	110, cool			0.7					
HEPES, 5 M NaCl	110, heat			1.8					
HEPES, 5 M NaCl	110, cool			1.0					
HEPES, 5 M NaCl	125, heat			1.7					
HEPES, 5 M NaCl	125, cool			1.1					
water	65, heat	3.0 ± 1.6							
water	65, cool	300							
water	96, heat	1.4	2.0						
water	96, cool	420	3.0						
water	100, heat		3.2 ± 1.6						
water	100, cool		2.7 ± 0.6						
water	110, heat	0.8	1.7 ± 0.7	3.1 ± 0.7					
water	110, cool	900	3.0 ± 1.7	1.2 ± 0.2					
water	115, heat		1.6 ± 0.2	2.3 ± 0.5					
water	115, cool		4.5	1.5 ± 0.1					
water	120, heat		1.6 ± 0.3	1.5 ± 0.2					
water	120, cool		2.3 ± 0.6	1.0 ± 0.3					
water	120, heat		1.7	1.8					
water	120, cool[f]		0.6	0.1				1.3 ± 0.6	
water	120, heat			4.7 ± 3.1				1.3 ± 0.6	
water	120, cool			1.4				5.6	

[a] Progress of the transition was monitored by low-angle time-resolved X-ray diffraction. [b] Aqueous phases consisted of Milli-Q water or 0.1 M Na-HEPES buffer, pH 7.4, with the NaCl concentrations indicated. [c] Temperature jump refers to the temperature of the heat gun air stream. Temperature jumps of 65, 90, 100, 110, 115, 120 and 125 °C resulted in final sample temperatures of 63, 88, 98, 108, 111, 119, and 121 °C. Heating is active while cooling is passive in air as explained in the text. [d] Transit time refers to the time it takes to undergo the indicated phase change as judged by visual inspection of the video-recorded time-resolved X-ray diffraction images. Transit time is the time interval between the first sighting of diffraction from the newly forming phase and the last detectable diffraction from the phase undergoing the transformation. The reported transit times are gross values as previously indicated (Caffrey, 1985). Transit times are shown as single-value determinations or as means ± standard deviations with number of replicates ranging from 2 to 9. [e] On the basis of the monoolein/water phase diagram of Hyde et al. (1984), a stable body-centered cubic (space group No. 12) phase at room temperature suggests that these samples were not fully equilibrated with the aqueous medium. Nonetheless, the t_T data are included in this table for completeness. [f] This sample was held at 120 °C for ca. 15 min before cooling was initiated.

perature transitions just described. With time and continued heating the transformation proceeds with the intensity in the low-temperature phase decreasing accompanied by a corresponding increase in scattered intensity from the high-temperature phase.

All of the transitions examined in this *T*-jump experiment show phase coexistence for finite time intervals. This may indicate that the transitions are first order and/or that a temperature gradient exist in the sample as it is being heated. This latter possibility has been shown to hold for hydrated lipid with the present sample geometry (Caffrey, 1985).

Upon cooling, the reverse process occurred with the notable exception that the CP4-to-BCC8 transition in ME is extremely slow (data not shown). Within any single-phase region the long spacing increased continuously with a decrease in temperature. The transitions themselves were discontinuous and exhibited phase coexistence for a finite time interval. It is reemphasized that throughout these experiments cooling is passive.

The process of heating and cooling was repeated many times, and the results described above were shown to be reproducible. It is noted, however, that due to its sluggish nature the reversibility of the intercubic transitions was not examined exhaustively in this study.

With the exception of the lamellar gel phase in ME, all other phases examined in this study have acyl chains in the "fluid" or disordered state and the wide-angle X-ray scattering peak is characteristically diffuse and is centered at ca. $(0.46\ nm)^{-1}$. Since TRXRD is relatively insensitive to diffuse scatter and since dramatic changes are not expected in this region of reciprocal space, the short-range order at the acyl chain level was not carefully monitored.

T-jump experiments were carried out with final temperatures ranging from 65 to 120 °C. The corresponding transit times (t_T) for each phase transition undergone by MO and ME in both the heating and cooling direction are presented in Tables III and IV. Transit time is defined as the time interval between the first sighting of diffraction from the newly forming phase and the last detectable diffraction from the phase undergoing the transformation. The transit times are, of course, gross values and include the time requires to (1) heat/cool the sample through the transition temperature range, (2) supply/remove the latent heat of the transition, and (3) undergo the transition, i.e., the intrinsic or net transit time. Thus, the intrinsic transit time is always less than the measured gross value.

(*1*) *Monoolein.* When dispersed in 0.1 M HEPES, pH 7.4, MO transforms from CP4 to H_{II} in the heating direction at 85 °C and subsequently melts at 106 °C (Figure 1B). At room temperature, and indeed down to −18 °C in the presence of an undercooled aqueous medium, CP4 is the "stable" phase. The kinetics of the CP4/H_{II} and the H_{II}/FI transitions were examined by applying *T*-jumps to 90, 100, and 110 °C (Table III). The transitions were complete in both heating and cooling directions in seconds, with the shortest t_T's observed following a *T*-jump to 110 °C.

Increasing NaCl concentration to 5 M in 0.1 M HEPES, pH 7.4, stabilized H_{II} at the expense of both the CP4 and the

Table IV: Transit Time of Various Thermotropic Phase Transitions Undergone by Aqueous Salt Dispersions of Monoelaidin in Response to a Temperature Jump[a]

NaCl concn[b] (M)	temperature jump[c] (°C)	transit time[d] (s)						
		lamellar gel — liquid crystal	X[e]	cubic (BC8)	cubic (P4)	H_{II}	FI	cubic (P4) — FI
0	90, heat	2.0	2.4	1.7				
0	90, heat	1.9	2.4	1.0				
0	116, heat	2.5	1.6	0.5				1.2
0	116, cool							0.9
0.5	90, heat		2.5	0.7				
0.5	90, heat		1.8	0.6				
0.5	107, heat		2.1	0.5	3.7			
0.5	107, heat		2.0	0.5	1.6			
0.5	107, cool			min[f]	1.2			
0.5	115, heat		1.7	0.5	1.0	1.0		
0.5	115, cool			min	1.4	1.0		
0.5	115, heat		2.0	0.5	0.9	1.2		
0.5	115, cool			min	1.0	0.6		
5	110, heat					1.6		
5	110, cool			min		0.9		
5	125, cool			min		1.0		

[a] Progress of the transition was monitored by low-angle time-resolved X-ray diffraction. [b] Aqueous phases consisted of Milli-Q water or 0.1 M Na-HEPES buffer, pH 7.4, with the NaCl concentrations indicated. [c] Temperature jump refers to the temperature of the heat gun air stream. Temperature jumps of 65, 90, 100, 110, 115, 120, and 125 °C resulted in final sample temperatures of 63, 88, 98, 108, 111, 119, and 121 °C. Heating is active while cooling is passive in air as explained in the text. [d] Transit time refers to the time it takes to undergo the indicated phase change as judged by visual inspection of the video-recorded time-resolved X-ray diffraction images. Transit time is the time interval between the first sighting of diffraction from the newly forming phase and the last detectable diffraction from the phase undergoing the transformation. The reported transit times are gross values as previously indicated (Caffrey, 1985). [e] The identity of this intermediate phase has not been established. See text for details. [f] The cubic (primitive, No. 4) to cubic (body centered, No. 8) transition is extremely slow when cooling is to room temperature (25–28 °C). However, when the sample is quenched in ice, conversion to the lamellar gel phase is rapid, occurring on the order of seconds.

FI phases (Figure 1B). Under present experimental conditions, only the H_{II}/FI transition was accessible to kinetic analysis and the T-jump experiment revealed a t_T in both heating and cooling directions of 1–2 s. It appears, therefore, that high salt concentration does not significantly alter the kinetics of this, the melting transition.

As noted previously, considerable difficulty was encountered in completely hydrating the MAG samples. In one such case, MO dispersed in HEPES buffer gave rise to the BCC12 phase at room temperature. This transformed to the CP4 and subsequently to the H_{II} phase upon heating. In a T-jump experiment the t_T of the BCC12/CP4 transition was found to be 1.3 s. However, upon cooling, the reverse transition was an order of magnitude slower, occurring with $t_T = 34$ s. While obtained with samples that were not fully equilibrated, these data are included in Table III for the sake of completeness.

In contrast to its phase behavior in HEPES buffer, MO dispersed in excess water occasionally (vide infra) existed at room temperature in the BCC8 phase. This gave way to the CP4 and subsequently to the H_{II} and FI phases upon heating. The kinetics of the BCC8/CP4 transition offered no surprises in the heating direction with t_T of ≤ 3 s, depending on the magnitude of the T-jump. The shortest t_T recorded for this transition was 0.8 s (Table III). Upon cooling, however, the reverse transition is extremely slow. The CP4 phase first undercools and then, at room temperature ($\sim$28 °C), slowly (5–15 min) converts to the BCC8 phase. Because of the tardy nature of this transition many of the T-jump experiments with MO in water were performed by starting from an undercooled CP4 phase.

The CP4-to-H_{II} phase transition also displayed a t_T on the order of seconds. A limiting value of 1.6–1.7 s was observed following T-jumps to 110, 115, and 120 °C regardless of whether the measurement was initiated in the BCC8 or the undercooled CP4 phase.

The H_{II}-to-FI melting transition was complete in a matter of seconds also with the shortest t_T observed following a T-jump to 120 °C. In one of the MO/water samples, which presumably was not fully hydrated, BCC12 was obtained as the room temperature phase. It transformed to the H_{II} phase with a t_T of 1.3 s. The subsequent H_{II}-to-FI transition was slow and variable ($t_T = 4.7 \pm 3.1$ s, $n = 3$).

In the cooling direction most of the transitions were fast, occurring in matters of seconds. Interestingly, a sample that had previously been brought to 120 °C by T-jump and held there for ca. 15 min displayed noticeably shorter t_T's of 0.1 and 0.6 s for the FI-to-H_{II} and the H_{II}-to-CP4 transitions, respectively. As noted above, the CP4-to-BCC8 transition is conspicuous by its extreme tardiness.

Without exception all of the MO transitions examined in this study appear to be two state to within the sensitivity limits of the TRXRD method. By two state is meant that at any point during the transition the TRXRD patterns reveal no more than two coexisting phases. It is emphasized, however, that the method is not sensitive to the presence of small amounts of diffuse scatter which, if present, is likely to go unnoticed (Caffrey, 1985; Caffrey & Feigenson, 1984). Furthermore, in the case of those phases with sharp low-angle diffraction patterns, generally the reflections remained sharp throughout the transition. This implies that long-range order is maintained during phase transformation as will be discussed below.

On two occasions during the course of the T-jump measurements, additional reflections of unknown origin were observed in what was expected to be single-phase regions of MO dispersed in either HEPES buffer or water (Figure 7). In the former case, just prior to the CP4-to-H_{II} transition, a faint, single sharp line emerged to the low-angle side of the CP4 (110) reflection during sample heating (Figure 7A-3). This was preceded by a dramatic broadening of the CP4 lines (Figure 7A-2). With time and continued heating the CP4 lines sharpened and the unidentified line faded to restore a typical sharp CP4-phase diffraction pattern immediately before transformation to the H_{II} phase.

In the case of MO in water, an unidentified diffraction line appeared during T-jump heating within the BCC8 phase. It emerged as a sharp, short-lived reflection between the (110) and (200) lines of the BCC8 phase (Figure 7B-2). As soon

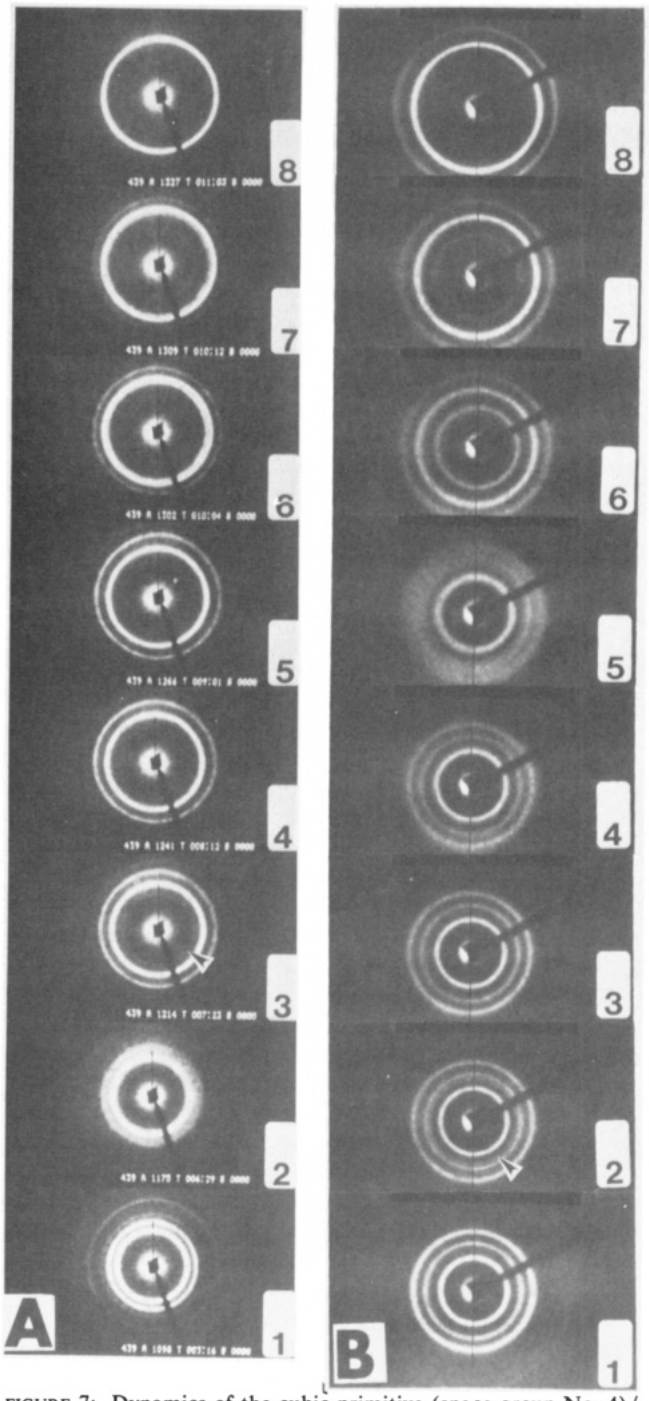

FIGURE 7: Dynamics of the cubic primitive (space group No. 4)/inverted hexagonal (A) and the cubic body-centered (space group No. 8)/cubic primitive (space group No. 4) (B) phase transformations in hydrated monoolein following a temperature jump to 100 °C. These low-angle patterns recorded by using time-resolved X-ray diffraction reveal the presence of transient, unidentified intermediate reflections (arrowheads in panels A-3 and B-2) and broadening of the single-phase reflections (panels A-2 and B-4,5,6) during the temperature-jump perturbation. Each photograph in the composite represents a single frame (33 ms) of the video-recorded, unprocessed images. Samples were dispersed in 0.1 M HEPES, pH 7.4 (A), and Milli-Q water (B). Elapsed time and in-sample temperature for the two sets are as follows: (A) 3.5 s, 25 °C (1); 7.0 s, 44 °C (2); 7.8 s, 53 °C (3); 8.4 s, 59 °C (4); 9.0 s, 65 °C (5); 10.1 s, 73 °C (6); 10.4 s, 74 °C (7); 11.1 s, 78 °C (8); and (B) 5.2 s, 33 °C (1); 6.1 s, 51 °C (2); 6.3 s, 55 °C (3); 6.6 s, 60 °C (4); 6.8 s, 63 °C (5); 7.1 s, 67 °C (6); 7.3 s, 70 °C (7); 8.0 s, 76 °C (8).

as this intermediate reflection faded, the BCC8 lines broadened considerably as the BCC8-to-CP4 transition was approached (Figure 7B-4,5,6). With time and continued heating, the diffraction pattern sharpened and the nascent CP4 phase emerged.

It is not known whether the transient differences associated with the BCC8 and CP4 phase reflections during *T*-jump heating arise as a result of an intrinsic disorder or a temperature gradient within the sample. Line broadening was not observed in the cooling direction.

A remarkable feature to emerge from the TRXRD measurements is the rate and degree to which lattice parameters within a given phase can change with time and temperature during *T*-jump heating and cooling. This is most evident in situations where a single-phase region exists over a wide temperature range. For example, at 5 M NaCl, the H_{II} phase of MO exists over a range of ca. 80 °C whereas in the absence of salt the temperature range of CP4-phase existence is on the order of 100 °C (Figure 1A). When *T*-jumps are applied through these various phases, the reciprocal space dimension of the diffraction patterns changes dramatically while maintaining the original one-phase pattern. For example, in the case of the H_{II} phase of MO at 5 M NaCl, $d_{10\bar{1}0}$ changed reversibly from 5.22 to 4.09 nm during the course of a 28 to 95 °C *T*-jump with maximum (initial) rates ($\Delta d_{10\bar{1}0}/\Delta t$) of −0.23 and 0.065 nm/s in the heating and cooling directions, respectively. For MO dispersed in HEPES alone the corresponding values in the CP4 phase for a 32 to 98 °C *T*-jump were $\Delta d_{100}^{\text{calcd}}/\Delta t = -1.22$ and 0.11 nm/s with limiting d_{100}^{calcd} values of 9.62 and 7.36 nm at 32 and ca. 80 °C, respectively. These latter initial rates translate into cubic unit cell length and volume reductions of 13%/s and 33%/s, respectively, during heating. It is remarkable that such rapid and extensive structural perturbations can take place without markedly disrupting the long-range order of the sample. Presumably aqueous-phase transport rates in these various phases must be sufficiently fast to accommodate such large volume changes.

(*2*) *Monoelaidin.* With one notable exception, all of the transitions examined in this study, whether in the heating or cooling direction, were fast, occurring on the time scale of seconds or less. The exception was the cooling transition within the cubic phase from CP4 to BCC8 as observed above with MO. Here the transition is complete on the order of tens of minutes. An exact transit time was not determined.

To within the sensitivity limits of the TRXRD method all of the ME transitions examined with one exception appear to be two state with no more than two phases coexisting at any one time. The exception was the L_α-to-BCC8 transition. Here a phase or possibly a number of phases appeared intermediate between the two limiting stable states. This held regardless of NaCl concentration or whether the transition was effected by slowly or rapidly raising sample temperature. For technical reasons the behavior of the system in the reverse direction upon cooling through the BCC8/L_α transition was not examined in this study. The usual method of restoring the sample to the low-temperature lamellar gel phase in preparation for a *T*-jump experiment was to quench the sample with ice. But because the conversion was so rapid (<30 s), it was not possible to follow the cooling process with the existing apparatus. This is presently under investigation.

As noted above, the intermediate, hereafter referred to as phase X, has not yet been identified. It is characterized by very low angle scattering which, when first formed from the L_α phase, is diffuse but sharpens up as temperature increases (Figures 5 and 6). Since phase X is also apparent in the slow temperature scan experiments, it should be possible to obtain high-resolution static X-ray diffraction photographs of this intermediate at various stages in its evolution. Worthy of note

in this context is that, with fully hydrated monomethylated dioleoylphosphatidylethanolamine (DOPE-Me), an as yet unidentified intermediate intervenes in the range 30 °C < T < 70 °C between the L_α and H_{II} phases. The intermediate displays an isotropic signal by ^{31}P NMR, and freeze–fracture electron microscopy indicates the presence of "lipidic particles". There may be some analogies between the intermediates seen with DOPE-Me (Gagne et al., 1985) and with ME since, in both cases, transitions are from the L_α to a nonbilayer phase.

During the L_α/X/BCC8 transition, the (110), (200), and (211) reflections of the BCC8 phase evolved from the low-angle scattering profile on the X intermediate. These reflections, when first formed, were visibly sharp. However, with time and continued heating, the (200) and (211) lines broadened slightly and subsequently sharpened up. The (110) reflection appeared to maintain its original degree of sharpness throughout. These observations hold for T-jumps to 90, 107, and 115 °C.

During the course of the T-jump experiments with ME in 0.5 M NaCl the (110) and (211) reflections of the CP4 phase appear to the low-angle side of, and very close to, the $(10\bar{1}0)$ and $(11\bar{2}0)$ lines of the H_{II} phase, respectively. Despite their proximity in reciprocal space, they are clearly resolved from one another, which serves to emphasize the lack of connectivity of the two phases under these conditions.

Midway through the H_{II}/CP4 cooling transition of ME the area between the (110) and (111) lines of the cubic phase displayed diffuse scatter which disappeared completely upon continued cooling.

Discussion

Since the pioneering work of Lutton, the physicochemical characterization of MAG/water systems has been the subject of considerable interest, especially in the food industry (Lutton, 1965; Hyde et al., 1984; Krog et al., 1985; Krog & Borup, 1973; Larsson, 1983, 1967; Lindblom et al., 1979; Ljusberg-Wahren et al., 1983; Larsson & Krog, 1973; Longley & McIntosh, 1983; Larsson et al., 1980; Ericsson et al., 1983; Ellis et al., 1969; Bohlin et al., 1985; Patton & Grey, 1979). Phase diagrams for both the MO/water and ME/water systems have been previously determined by using polarized light microscopy (PLM; Lutton, 1965; Krog et al., 1985; Ljusberg-Wahren et al., 1983). The transition temperatures observed in this work by TRXRD are in agreement with the literature values. PLM does not, however, distinguish the different cubic modifications, and the present report is the first to identify and to structurally characterize the various cubic phases occurring in the ME system. These include the BCC8 and the CP4 phases. Both of these phases, along with a BCC12 phase, were observed (Figure 1, Table II) in the MO system.

Structural Parameters. Structural characterization of hydrated MO by X-ray diffraction has been performed by Larsson (1983) and by Longley and McIntosh (1983). Both of these measurements were made in water at 22 °C. Larsson (1983) reported a unit cell dimension (a_{calcd}) value of 9.08 nm for the CP4 phase at 39.87% (w/w) water, while the corresponding value in excess water obtained by Longley and McIntosh (1983) was 10.5 nm. Data presented in Table I for MO in excess 0.1 M HEPES, pH 7.4, provide an a_{calcd} value of 9.83 nm at 13 °C. The same data in Table I demonstrate that salt depresses a_{calcd}, and the TRXRD results in Figure 3 show that the thermal lattice coefficient in this phase is of negative sign. Taken together, these two facts suggest that correcting the present a_{calcd} value for salt and high temperature will operate in opposite directions.

A direct comparison between the structural parameters of common phases in MO and ME is not possible because measurements were made at very different temperatures in the two systems. However, the effect of salt on the lattice parameters of the various mesomorphic phases was similar as was the thermotropic sequence of phases, which proved independent of salt concentration.

Salt Effects. It is interesting to note that when measurements were made at comparable temperatures, salt had a minimal effect on the lattice parameters of the lamellar phases. In contrast, salt depressed the lattice parameter of the various nonbilayer phases and the characteristic d spacing of the FI phase.

In the absence of NaCl, the dominant phase in fully hydrated MO at low temperatures was CP4 (Figure 1A). At higher temperatures the H_{II} phase appeared, followed by the FI. The addition of salt stabilizes the H_{II} at the expense of both FI and cubic phases, and at 5 M salt, it is the dominant phase (Figure 1A). The MO/water temperature–composition phase diagrams of Lutton (1965) and of Krog et al. (1985) show that reducing water content isothermally favors the FI over the cubic and H_{II} phases. High salt alters water polarizability as evidenced by its ability to reduce the dielectric constant of bulk water from 79 in the absence of salt to 55 in 2 M NaCl (Hasted, 1973). This gives rise to an effective dehydration, which explains part of the salt effect on MO phase behavior observed in the present work. A salt-induced dehydration, however, does not account for its enormous stabilizing influence on the H_{II} phase since the literature MO/water phase diagrams show this phase to exist over a relatively narrow temperature range and to be destabilized completely at less than 10% (w/w) water (Lutton, 1965; Krog et al., 1985).

The MAGs are neutral lipids remaining totally uncharged over a wide pH range. Thus, the salt effect cannot be one of electrostatic screening. Moreover, screening of this sort in charged lipids is usually complete by 2 M salt (March, 1983). In the present case, the stabilizing influence of salt continues unabated up to 5 M salt. It seems likely, therefore, that additional effects such as hydrogen bonding, head group–water interactions, dielectric permittivity, etc., all of which are sensitive to salt concentration (and to temperature; Franks, 1985; Hasted & Shakidi, 1976; Seddon et al., 1983; Hasted, 1973), are contributing to the observed effect on NaCl on MAG mesomorphism.

The sequence of phases observed in fully hydrated ME in the absence of NaCl with increasing temperature was as follows: lamellar gel, L_α, unidentified intermediate (phase X), BCC8, CP4, and FI. The corresponding sequence observed by Lutton (1965) and by Krog et al. (1985) was crystalline, lamellar, cubic, and FI without any details as to the identity of the various lamellar and cubic modifications. The crystalline phase was not observed in the present study presumably because it forms slowly and at low temperatures. The ME samples used in these experiments were usually quenched in ice from room temperature or above before measurement, a treatment likely to produce the observed long-lived, metastable lamellar gel phase. The stability of the latter was not investigated in this study. It is interesting to note that neither Lutton (1965) nor Krog et al. (1985) described any unusual behavior other than phase coexistence between the lamellar and the cubic phases. In the present study this region was occupied by an, as yet, unidentified intermediate or possibly series of intermediate phases with disordered acyl chains and considerable long-range order (vide infra).

The addition of salt to the hydrated ME system stabilizes the lamellar gel phase with a maximal effect at ≥2 M NaCl. The most dramatic effect of salt in this sytem, however, was the expression of the H_{II} phase at low salt, which at the expense of the L_α, X, and FI phases, became the dominant phase at 5 M NaCl. In this regard then, both MO and ME behave similarly. A careful investigation of the ME cubic/FI transition region in the absence of added NaCl was carried out to screen for the presence of H_{II} phase over a narrow temperature range to no avail. Thus, a finite salt concentration over and above that supplied by the buffer is required for expression of the H_{II} phase in the present system.

The ME/water temperature–composition phase diagrams established by Lutton (1965) and by Krog et al. (1985) illustrate that, as with the MO system, isothermal dehydration stabilizes the FI and lamellar over the cubic phase in a wide range of temperatures. These data suggest that part of the influence of salt on the H_{II}/FI phase transition observed in the present study might be accounted for by an effective salt-induced dehydration. This, however, is not consistent with the effect of salt on the lamellar/cubic transition except over a very limited hydration range [Figure 3b in Krog et al. (1985)]. Furthermore, expression of the H_{II} phase and its enhanced stability at high salt cannot be related to the aforementioned ME phase diagram studies because it does not appear under the prevailing experimental conditions. Thus, as with MO, the observed salt effects are likely attributable to a number of factors including dehydration, head group–water interactions, hydrogen bonding, and bulk water dielectric permittivity.

Seddon et al. (1983), working with a variety of phosphatidylethanolamines, noted that NaCl dramatically depressed the lamellar/hexagonal phase transition temperature and raised the lamellar chain-melting temperature but to a lesser extent. Our data are consistent with these results although a direct lamellar/hexagonal transition was not observed in the ME system.

The thermotropic phase properties of hydrated MO and ME, which differ only in isomeric type of unsaturation (cis vs. trans, respectively), are quite disparate in the absence of NaCl (cf. Figure 1). However, if we compare the phase sequence and transition temperatures of MO at 5 M NaCl with those of ME at 1 M NaCl, almost identical behavior is observed in the temperature range of 50–120 °C. Thus, the acyl chain configurational effects can be experimentally normalized by suitably adjusting salt concentration.

Sorbitol Effects. To determint if the effects of added salt on the phase properties of MAGs could be mimicked by a low molecular weight organic solute, the thermotropic phase behavior of ME in excess 5 M sorbitol (in 0.1 M HEPES, pH 7.4) was examined (data not shown). Unlike NaCl, sorbitol stabilized the FI phase down to 85 °C. Furthermore, the structural parameters and acyl chain packing characteristics of the lamellar gel phase are distinctly different from those observed with salt although chain melting occurred at approximately the same temperature as in 2–5 M NaCl. In the presence of sorbitol, the phases intervening between the lamellar gel and the FI were not identified because of the complex nature of the corresponding low-angle diffraction pattern. These results suggest that the mesomorphic response of ME to added solute is not simply colligative and emphasize the importance of specific solute–lipid–solvent interactions.

Monoacylglyceride Hydration. As noted in the introduction, difficulties were encountered in preparing homogeneous samples of MAGs, MO in particular, at less than full hydration following standard procedures. The probem is that, upon incubating the lipid with water for extended periods (days to weeks), accompanied by high/low-temperature cycling treatments and by centrifugation to effect mixing, different mesomorphic phases were observed by TRXRD in different parts of the sample. Experiments are now in progress to examine the nature and dynamics of MO hydration (Caffrey, 1987b). Despite the problems, some interesting results were obtained with these samples which have been described under Results.

Transition Kinetics and Mechanism. Eight different mesomorphic phase transformations have been examined in the present MAG/water systems which include ME and MO. These transitions are the lamellar gel/L_α, L_α/X/BCC8, BCC8/CP4, CP4/H_{II}, H_{II}/FI, CP4/FI, BCC12/CP4, and BCC12/H_{II}. They differ in terms of the structural parameters that undergo change as well as the dimensionality of the periodicity which ranges from zero in the FI to one in the lamellar to two in the H_{II} to three in the cubic phase. In certain cases, the transition does not involve a change in dimensional periodicity as in the chain-melting and the intercubic transitions. In others, the change is extreme, requiring, for example, a large topological transformation from an isotropic fluid to the complex three-dimensional lattice of the cubic phase. This study shows that all of the heating transitions are fast, occurring on the order of seconds. In the cooling direction all but two of the transitions are equally fast. The exceptions are the CP4-to-BCC12 and the CP4-to-BCC8 transitions, which do not involve changes in dimensional periodicity. The sequence of events in these slow transitions is first an undercooling of the CP4 phase followed by a slow conversion at room temperature to the low-temperature phase.

All of the transitions studied were found to be repeatable and reversible, although in the majority of cases, hysteresis and/or undercooling effects were observed. The transitions were two state to within the sensitivity limits of the TRXRD method with no more than two phases coexisting at any point during the transition. As noted previously (Caffrey, 1985), transition intermediates that do not accumulate to significant levels or that lack sufficient long-range order may go undetected due to the limited sensitivity of the present TRXRD method. The one exception to this was the L_α-to-BCC8 transition in which an unidentified intermediate, referred to as phase X, appeared during the course of the heating transformation.

All of the transitions were discontinuous in that the low-angle diffraction patterns from the two adjacent phases were clearly resolved and did not grow continuously one from the other. The one possible exception to this generalization was the BCC8/CP4 transition. Here the (110) and (111) reflections of the newly forming CP4 appeared to grow directly from the (200) and (211) reflections of the decaying BCC8 phase while the BCC8 (110) line gradually faded. This observation holds true for both MO and ME. It is emphasized, however, that these results are based on the TRXRD measurements and that high-resolution static (or dynamic) measurements may reveal small differences in the *d*-spacing values of these two sets of low-angle reflections. If the two sets of reflections are indeed continuous through the transition, a structural connectivity between the BCC8 and CP4 phases may exist. Verification awaits elucidation of the three-dimensional structures of these two mesomorphs.

Most of the transitions examined in this study were two state with well-defined and sharp diffraction patterns from the two transforming phases coexisting during the *T*-jump-induced

transition. This implies that long-range order was maintained in each phase during the transformation process, a remarkable result in light of the complexities of the various transitions undergone. These involve interconversions of structures periodic in zero (fluid isotropic), one (lamellar), two (hexagonal), and three (cubic) dimensions, structural rearrangements at the acyl chain packing level, and changes in the relative volume fraction of the lipid and water components. The maintenance of line sharpness throughout the transition therefore suggests that large numbers of lamellae, hexagonal rods, or extensive three-dimensional lipid aggregates undergo the transformation together in a highly cooperative manner and, further, that long-range order is rapidly established in the nascent phase regardless of the direction (cooling or heating) of approach. These results also imply that within any given phase a high degree of coupling is maintained from one lipid compartment to the next through the intervening aqueous medium.

On a number of occasions during the course of the *T*-jump measurements transient line broadening plus the transient appearance of additional low-angle reflections of unknown origin was observed in the single-phase region just below the transition. These results apply to the heating direction only. It is possible that the broadening effect is an apparent one, arising from transient temperature gradients known to exist in the samples during *T*-jump heating (Caffrey, 1985). It may also be that the rate of aqueous-phase transport within the phase is not sufficient and that the lattice disrupts temporarily to relieve accumulated strain.

The BCC8 phase of hydrated MO has not been previously reported. From the dynamic measurements carried out in the course of this study, we know that BCC8 re-forms, but slowly, from the CP modification (Tables II and III). It is possible in other studies of the MO system that the thermal history of the sample plus the conditions of measurement were such that the hydrated lipid was kinetically trapped in the CP4 phase (Longley & McIntosh, 1983; Larsson, 1983; Hyde et al., 1984). Indeed, as noted under Results, many of the *T*-jump experiments with the MO/water system were performed by starting with an undercooled CP4 phase because of the sluggish nature of the CP4-to-BCC8 transition. As noted by Luzzati et al. (1986), there may be associated with cubic-phase metastability in biological systems a protective advantage to endure extreme fluctuations in ambient temperatures.

The BCC8 phase was observed under conditions designed to "ensure" full hydration of the lipid. In a separate but related study (Caffrey, 1987b), which will be reported on more completely at a later date, the dynamics of MO hydration was examined. Pure MO was brought into contact with water, and the diffusional flow of water into the lipid at a fixed temperature was followed by TRXRD. Samples prepared in this way revealed the following mesomorphic phase sequence beginning from the water-rich end: BCC8, CP4, BCC12, L_α, and FI. However, the BCC8 phase was not consistently seen. The precise conditions that favor its appearance have not been identified. An identical sequence but lacking the BCC8 phase is to be found in the MO/water phase diagram of Hyde et al. (1984). This unusual behavior may be related to metastability and/or to the extremely small energy difference between the various cubic-phase modifications (vide infra).

Cubic Infinite Periodic Minimal Surfaces. The three cubic modifications observed in the present study of hydrated MO provide examples of the three fundamental cubic infinite periodic minimal surfaces (IPMS's) in a single lipid system. An IPMS is an intersection-free surface periodic in three dimensions with an average curvature that is everywhere zero. An IPMS divides space into two equivalent, interpenetrating three-dimensional networks that remain unconnected throughout their full extent. In the hydrated lipid systems the IPMS is viewed as lying at the center of a single, continuous lipid bilayer where the two monolayers meet and compartmentalizes the two interwoven water-filled labyrinths with the polar lipid headgroups lining the two water/hydrocarbon interfaces.

The three fundamental cubic IPMS's are referred to as being of the diamond (D), the gyroid (G), or the Schwarz' (P) type and correspond respectively to the CP4, BCC12, and BCC8 cubic space groups. The three surfaces are mutually accessible via certain mathematical transformations which involve a bending of the surface without a change in curvature. As a result, the transitions are energetically inexpensive. On the basis of DSC measurements, Hyde et al. (1984) have estimated the enthalpy change associated with the BCC12/CP4 transition in MO/water to be less than 0.003 kcal/mol, which is some 2 orders of magnitude lower than that associated with most lipid mesomorphic transitions. As suggested by Hyde and Andersson (1985), a common example of a mathematical transformation of the type described is the Martensite transition which occurs when steel is quenched. The transition is diffusionless and is extremely fast, oftentimes aproaching the speed of sound. Relating this to the present study, it is noted that the intercubic transitions are indeed rapid in the heating direction with $t_T \leq 2$ s. However, in the cooling direction all of these transitions are slow with t_T some 1–3 orders of magnitude greater than observed in the heating direction. It may be that the sluggish nature of the cooling transitions derives from a slow expansion of the cubic lattice to the precise value with which the newly forming low-temperature cubic phase can exist in equilibrium for that particular overall lipid/water composition and the range of temperatures over which the transition occurs. A resolution of this issue necessitates the construction of a detailed MO/water temperature–composition phase diagram in conjunction with carefully performed dynamic TRXRD measurements.

As noted previously, the speed of a transition may reflect more the ease with which nucleation and growth and water equilibration between coexisting phases occur than the complexity of the molecular rearrangements undergone during the transition (Caffrey, 1985). Moreover, it is generally held that heating transitions starting from a solid, crystal, or liquid-crystalline state are more rapid than their liquid counterparts because of the higher concentration of defects which provide nucleation sites for new-phase growth.

ACKNOWLEDGMENTS

I thank B. W. Batterman (National Science Foundation Grant DMR81-12822), D. H. Bilderback, G. W. Feigenson (National Institutes of Health Grant HL-18255), and the entire CHESS and MacCHESS staff for their invaluable help and support. I further thank Ellen Patterson for carefully typing the manuscript, J. K. Moffat for use of the sealed-tube and rotating anode X-ray sources (National Institutes of Health Grants GM29044 and RR-01646), W. W. Webb for making available the Grinnell image processing system, and Dave Siegel and Sol Gruner for critically reading the manuscript.

REFERENCES

Bohlin, L., Ljusberg-Wahren, H., & Miezis, Y. (1985) *J. Colloid Interface Sci. 103*, 294–295.

Caffrey, M. (1984) *Nucl. Instrum. Methods Phys. Res., Sect. A 222*, 329–338.

Caffrey, M. (1985) *Biochemistry 24*, 4826–4844.

Caffrey, M. (1987a) *Biochim. Biophys. Acta 896*, 123–127.
Caffrey, M. (1987b) *Biophys. J. 51*, 444a.
Caffrey, M., & Feigenson, G. W. (1981) *Biochemistry 20*, 1949–1961.
Caffrey, M., & Bilderback, D. H. (1983) *Nucl. Instrum. Methods Phys. Res. 208*, 495–510.
Caffrey, M., & Bilderback, D. H. (1984) *Biophys. J. 45*, 627–631.
Caffrey, M., & Feigenson, G. W. (1984) *Biochemistry 23*, 323–331.
Caffrey, M., & Hing, F. S. (1987) *Biophys. J. 51*, 37–46.
Ellis, B., Lawrence, A. S. C., McDonald, M. P., & Peel, W. E. (1969) in *Liquid Crystals and Ordered Fluids* (Johnson, J. F., & Porter, R. S., Eds.) Vol. 1, pp 277–288, Plenum, New York.
Ericsson, B., Larsson, K., & Fontell, K. (1983) *Biochim. Biophys. Acta 729*, 23–27.
Franks, F. (1985) *Biophysics and Biochemistry at Low Temperatures*, Cambridge University Press, New York.
Gagné, J., Stamatatos, L., Diacovo, T., Hui, S. W., Yeagle, P. L., & Silvius, J. R. (1985) *Biochemistry 24*, 4400–4408.
Hasted, J. B. (1973) *Aqueous Dielectrics*, Chapman & Hall, London.
Hasted, J. B., & Shahidi, M. (1973) *Nature (London) 262*, 777–778.
Holman, J. P. (1976) *Heat Transfer*, 4th ed., McGraw-Hill, New York.
Hyde, S. T., & Andersson, S. (1985) *Z. Kristallogr. 170*, 225–239.
Hyde, S. T., Andersson, S., Ericsson, B., & Larsson, K. (1984) *Z. Kristallogr. 168*, 213–219.
International Tables for X-ray Crystallography (1968) Vol. II, p 122.
Kirk, G. L., Gruner, S. M., & Stein, D. L. (1984) *Biochemistry 23*, 1093–1102.
Krog, N. J., Riisom, T. H., & Larsson, K. (1985) in *Encyclopedia of Emulsion Technology: Applications* Becher, P., Ed.) Vol. 2, pp 321–365, Marcel Dekker, New York.
Larsson, K. (1967) *Z. Phys. Chem. Mem. Folge 56*, 173–198.
Larsson, K. (1983) *Nature (London) 304*, 664.
Larsson, K., & Krog, N. (1973) *Chem. Phys. Lipids 10*, 177–180.
Larsson, K., Fontell, K., & Krog, N. (1980) *Chem. Phys. Lipids 27*, 321–328.
Lindblom, G., Larsson, K., Johansson, L., Fontell, K., & Forsen, S., (1979) *J. Am. Chem. Soc. 101*, 5465–5470.
Ljusberg-Wahren, H., Herslöf, M., & Larsson, K. (1983) *Chem. Phys. Lipids 33*, 211–214.
Longley, W., & McIntosh, T. (1983) *Nature (London) 303*, 612–614.
Lutton, E. S. (1965) *J. Am. Oil Chem. Soc. 42*, 1068–1070.
Luzzati, V. (1968) In *Biological Membranes, Physical Fact and Function* (Chapman, D., Ed.) Vol. 1, pp 71–123, Academic, New York.
Luzzati, V., Gulik, A., Gulik-Krzywicki, T., & Tardieu, A. (1986) in *Lipids and Membranes: Past, Present and Future* (Op den Kamp, J. A. F., Roelofsen, B., & Wirtz, K. W. A., Eds.) pp 137–151, Elsevier, Amsterdam.
Marsh, D. (1983) in *Supermolecular Structure and Function* (Pifat, G., & Herak, J. N., Eds.) pp 127–128, Plenum, New York.
Pagano, R. E., Cherry, R. J., & Chapman, D. (1973) *Science (Washington, D.C.) 181*, 557–559.
Patton, J. S., & Carey, M. C. (1979) *Science (Washington, D.C.) 204*, 145–148.
Seddon, J. M., Cevc, G., & Marsh, D. (1983) *Biochemistry 22*, 1280–1289.
Shipley, G., Green, J. P., & Nichols, B. W. (1973) *Biochim. Biophys. Acta 311*, 531–544.
Siegel, D. P. (1984) *Biophys. J. 45*, 399–420.
Wieslander, A., Christiansson, A., Rilfors, L., & Lindblom, G. (1980) *Biochemistry 19*, 3650–3655.